The FASEB Journal

FASEB
Federation of American Societies for Experimental Biology

RESEARCH ARTICLE OPEN ACCESS

Inside-Out IP_3-Mediated G Protein-Coupled Receptor Activation Drives Intercellular Ca^{2+} Signaling in the Vascular Endothelium

C. Buckley | X. Zhang | M. D. Lee | C. Wilson | J. G. McCarron

Strathclyde Institute of Pharmacy and Biomedical Sciences, University of Strathclyde, Glasgow, UK

Correspondence: J. G. McCarron (john.mccarron@strath.ac.uk)

Received: 7 February 2025 | **Revised:** 24 June 2025 | **Accepted:** 30 June 2025

Funding: This work was supported by British Heart Foundation (BHF), RG/F/20/110007.

Keywords: blood vessels | calcium signaling | calcium waves | cell communication | endothelium | GPCR | vascular tone

ABSTRACT

The endothelium's control of nearly all vascular function relies on rapid intercellular communication to coordinate cellular activity across scale. A key form of intercellular communication arises from the regenerative propagation of IP_3-evoked Ca^{2+} signals from cell to cell, which regulate vessel tone, modulate vascular permeability, and determine immune responses. Despite their importance, the mechanisms by which regenerative propagation of IP_3-evoked Ca^{2+} signals occurs are poorly understood. Here, in intact resistance arteries, precision photolysis of IP_3 combined with high-resolution mesoscale imaging, targeted drug application, and advanced analytical techniques was used to determine the mechanisms underlying regenerative propagation of IP_3-evoked Ca^{2+} signals in the endothelium. Elevated IP_3 in the initiating cell triggers a noncanonical inside-out signaling mechanism that leads to transcellular activation of a $G_{\alpha q/11}$-coupled receptor in a neighboring (receiving) cell. This, in turn, initiates canonical outside-in signaling via PLC, leading to the hydrolysis of PIP_2 and production of IP_3. This process creates a regenerative, IP_3-dependent signaling cascade operating between adjacent cells. Notably, neither Ca^{2+} nor IP_3 diffusion through gap junctions plays a significant role in intercellular communication. Our findings uncover a previously unrecognized mechanism of endothelial communication, in which noncanonical IP_3-driven transcellular activation of G protein-coupled receptors sustains a regenerative signaling loop, highlighting a novel framework for intercellular coordination in the vascular endothelium.

1 | Introduction

The endothelium, a critical regulator of vascular function, relies on precise intercellular communication to manage signals that control blood vessel diameter, permeability, angiogenesis, and immune responses. A fundamental mechanism underlying this communication is the regenerative propagation of IP_3-evoked Ca^{2+} signals among cells to enable coordination of endothelial activity. However, the mechanisms triggering regenerative IP_3 production and subsequent signal propagation are poorly understood, limiting our ability to address vascular dysfunctions associated with diseases like hypertension and neurodegenerative conditions. We describe a novel mechanism for intercellular communication, whereby noncanonical IP_3 activation of a transcellular G protein-coupled receptor (GPCR) drives regenerative IP_3 production in neighboring cells.

Cardiovascular function is monitored and adjusted by the endothelium in response to a multitude of incoming signals that act on endothelial cells. The endothelium manages the signaling load by using cells that are specialized to detect specific stimuli, which then communicate with neighboring endothelial cells to transmit information and coordinate changes in endothelial function across scale [1]. This "transcellular"

This is an open access article under the terms of the Creative Commons Attribution License, which permits use, distribution and reproduction in any medium, provided the original work is properly cited.

© 2025 The Author(s). *The FASEB Journal* published by Wiley Periodicals LLC on behalf of Federation of American Societies for Experimental Biology.

information transfer between endothelial cells is encoded in concentration levels of second messengers such as IP_3 and Ca^{2+}.

An important mechanism driving increases in intracellular Ca^{2+} is the opening of IP_3 receptors (IP_3Rs) on internal stores, principally the endoplasmic reticulum. This canonical signaling cascade is typically initiated by ligand binding to GPCRs on the outer membrane of cells, inducing a conformational change in the G protein which allows the subunit to dissociate and initiate downstream signaling pathways. There are four prominent classes of G protein families, with $G\alpha_{q/11}$ being the primary subfamily involved in endothelial IP_3-mediated Ca^{2+} release [2, 3]. Blood vessel activators that act on the endothelium, for example, acetylcholine (ACh), bind $G\alpha_{q/11}$ GPCRs, such as the M3 muscarinic receptor, stimulating phospholipase Cβ (PLCβ) to hydrolyze membrane-bound phosphatidylinositol-4,5-biphosphate (PIP_2). PIP_2 splits into diacylglycerol (DAG) and inositol-1,4,5-triphosphate (IP_3). The free IP_3 binds and opens IP_3Rs on the endoplasmic reticulum, allowing Ca^{2+} release from the internal stores.

Alterations in Ca^{2+} concentrations within single endothelial cells are translated into endothelial-wide coordinated responses by the propagation of Ca^{2+} gradients ("Ca^{2+} waves") between cells [4]. The mechanisms which act to scale local intracellular signals to drive extended cell–cell communication remain surprisingly obscure and contentious. Notwithstanding, traditional hypotheses propose that signaling occurs in one of two ways; paracrine diffusion of molecules like ATP, or by the transcellular movement of IP_3 through gap junctions. Paracrine diffusion entails the release and diffusion of a factor into the extracellular space to bind to a receptor on the plasma membrane of a neighboring cell, triggering downstream intracellular signaling [5]. In the case of diffusion through gap junctions, IP_3 [6–8] flux will be driven between cells by the electrochemical driving force acting on the inositide to trigger Ca^{2+} release from the internal stores in neighboring cells [9]. Since IP_3 is a trivalent anion, in addition to changes in the concentration gradient of the inositide, changes in transmembrane potential should exert influence in the transcellular flux of IP_3 between coupled cells. However, both models (paracrine signaling and gap junction coupling) fail to fully explain the dynamics observed in the vascular endothelium. For example, paracrine communication is unlikely to transmit significant signaling against the direction of blood flow.

Recently, we proposed that a novel mechanism accounts for cell communication [10]. In the vascular endothelium, IP_3 is sufficient to evoke a regenerative Ca^{2+} wave propagation across cells in direct physical contact, without relying on diffusion of either IP_3 or Ca^{2+} via gap junctions. Instead, IP_3 appears to activate an unidentified PLC "bridge" that mediates signal transmission between neighboring adjacent cells. The bridge either directly or indirectly activates PLC, leading to the breakdown of PIP_2 and the generation of IP_3. Consequently, IP_3 mediates IP_3 production in adjacent cells to regeneratively propagate the Ca^{2+} signal. The question arises as to how IP_3 generates IP_3 production, and the role played by IP_3 receptors. Since agonist-induced IP_3 production is initiated by GPCR activation, we hypothesized that IP_3 may activate a GPCR to facilitate IP_3 generation during the propagation of endothelial Ca^{2+} waves.

Here, using a cutting-edge imaging approach that allows precise activation or deactivation of specific subgroups of cells in intact resistance arteries, we demonstrate that an increase in IP_3 in one cell activates $G\alpha_{q/11}$-coupled GPCRs in neighboring cells. This triggers PLC-mediated hydrolysis of PIP_2 into IP_3 in neighboring cells, enabling regenerative, IP_3-driven signal transmission between endothelial cells. Importantly, this propagation does not depend on gap junctions or electrochemical gradients.

These findings reveal a previously unrecognized pathway for intercellular communication and provide critical insights into the complexity of mechanisms driving vascular signaling.

2 | Materials and Methods

2.1 | Animals

All animal husbandry and sacrifice were carried out in accordance with the prior approval of the University of Strathclyde Animal Welfare and Ethical Review Body and under relevant UK Home Office Regulations (Schedule 1 of the Animals [Scientific Procedures] Act 1986, UK). Strathclyde biological procedures unit is a conventional facility that undertakes FELASA quarterly health monitoring. Animal studies are reported in compliance with the ARRIVE guideline [11].

Male Sprague–Dawley rats (10–12 weeks old; 250–300 g), from an in-house colony, were used for the study. The animals were housed 3 per cage and the cage type was North Kent Plastic model RC2F with nesting material "Sizzle Nest." A 12:12 light dark cycle was used with a temperature range of 19°C–23°C (set point 21°C) and humidity levels between 45% and 65%. Animals had free access to fresh water and SDS diet RM1 (rodent maintenance). The enrichment in the cages was aspen wood chew sticks and hanging huts. Animals were euthanized by cervical dislocation and death confirmed by exsanguination. The mesenteric bed was removed. All experiments were performed using first- to third-order mesenteric arteries. Controls and experimental treatments were carried out in the same tissue, so blinding and randomization were not used. Group sizes were designed to be equal.

2.2 | Mesenteric Artery Preparation and Mounting

To prepare *en face* blood vessel preparations, dissected arteries were cleaned of fat and connective tissue and cut open longitudinally to expose the endothelial layer. Arteries were then pinned flat in custom-designed baths, with a Sylgard base, using 50 μm diameter pins. Dissection and experiments were carried out in a physiological saline solution (PSS: 145 mM NaCl, 2 mM MOPS, 4.7 mM KCl, 1.2 mM NaH2PO4, 5 mM Glucose, 0.02 mM EDTA, 1.17 mM MgCl, 1 mM CaCl, pH 7.4). In some experiments, Ca^{2+} free PSS (145 mM NaCl, 2 mM MOPS, 4.7 mM KCl, 1.2 mM NaH2PO4, 5 mM Glucose, 0.02 mM EDTA, 2.34 mM MgCl,1 mM EGTA, pH 7.4) and high K^+, Ca^{2+} free-PSS (2 mM

MOPS, 134.4 mM KCl, 1.2 mM NaH2PO4, 5 mM Glucose, 0.02 mM EDTA, 1.17 mM MgCl, pH 7.4) were used.

Endothelial cells were loaded with the Ca^{2+} indicator dye Cal520/AM (5 μM in PSS with DMSO and 0.02% Pluronic F-127) for 30 min at 37°C and then mounted in a custom-designed flow chamber [12].

2.3 | Endothelial Patch Isolation

Mesenteric arteries (first to third order) were dissected, the fat removed, and cut open longitudinally. Any blood that remained on the endothelial surface was carefully removed. Arteries were cut into five strips of approximately 2 mm length, suspended in PSS with collagenase (Type 2, 256 units/mg, 2 mg.mL^{-1}), and enzymatically digested in a water bath at 37°C for 45 min. The supernatant was removed, and a wide-bored, fire-polished glass pipette was used to gently triturate arteries and isolate the endothelial cell patches. Patches were transferred to an 8-well chamber slide (μ-slides; Ibidi, Germany) for 3 h before fixation for immunocytochemistry.

2.4 | Image Acquisition

2.4.1 | Imaging System 1

A Nikon Eclipse FNI upright microscope equipped with a Nikon Fluor 16X 0.8 NA water immersion objective lens and a pE-4000 CoolLED system (365/490/550/635 nm excitation) and a quad DAPI/FITC/TRITC/Far Red filter set. Images were acquired using a Photometrics Evolve 13 EMCCD camera (1024 × 1024). All images were acquired using MicroManager v2 [13] for 2 min at 10 Hz.

The microscope rig was equipped with a hydrostatic pressure ejection system (Pneumatic PicoPump PV820, World Precision Instruments, Sarasota, FL, USA), allowing focal application of drugs from a puffer pipette that was positioned ~50 μm above the surface of the blood vessel, perpendicular to the direction of the flow. See "Localized Pressure Ejection Experiments" section.

2.4.2 | Imaging System 2

A Nikon Eclipse TE300 inverted microscope fitted with a CoolLED pE-300 LED illumination system (400/490/550 nm excitation) and custom designed DAPI/FITC/TRITC filter set. A 40X 1.3 NA Nikon S Fluor oil-immersion objective lens was used for Ca^{2+} imaging experiments, and a 100X 1.3NA Nikon S-Fluor lens for imaging immunocytochemistry on endothelial patches. Images were acquired using an Andor iXon EMCCD camera (1024 × 1024) and MicroManager v1.44 [14].

2.5 | Acetylcholine Application

In experiments where acetylcholine (ACh) was used to elicit Ca^{2+} responses, directional flow (1.5 mL.min^{-1}) was used throughout the experiment. The directional flow consisted of either PSS (control) or ACh (100 nM) in PSS. After ACh application, arteries were washed (with PSS) for 10 min to ensure ACh removal, followed by a 5 min rest period before subsequent recordings.

To visualize Ca^{2+} activity, images were created by calculating $\Delta F/F_0$ for each image in the recording. A maximum intensity projection of 10 s (100 frames) following ACh application was taken and presented using a time-correlated colormap.

2.6 | Localized Uncaging

In experiments in which endothelial Ca^{2+} responses were evoked by photolysis of caged IP_3, the endothelium was loaded with Cal520/AM (5 μM in PSS with DMSO and 0.02% Pluronic F-127) and a membrane-permeant Ins(1,4,5) P3-caged IP_3 (5 μM; cIP_3) for 30 min at 37°C [15, 16].

Laser photolysis of cIP_3 was achieved using a Rapp OptoElectronic DL-Series UV (375 nm) laser coupled into a Firefly system, with a UGA-42 scanner, to set the uncaging region via the software. This system was mounted onto Imaging System 1. The UV photolysis light was first passed through an attenuating neutral density filter (1% transmission) and used at a power such that it was 2 mW before loss as it traveled through the optics. The region of interest was determined using the acquisition frames over which the laser had been used. In this experimental setup, experiments blocking PIP_2 generation used LY294002 (300 μM) and wortmannin (50 μM), and GPCR function was inhibited using YM254890 (1 μM), or FR900359 (5 μM), or NF 449 (1 μM), or Gallein (5 μM), or Pretussis toxin (PTX 100 ng.ml^{-1}).

In other experiments, flash photolysis of cIP_3 was achieved using a Rapp Optoelectronics flash lamp (00-325-JML-C2) at 200 V, which produced light of ~1 ms duration. This system was mounted onto Imaging System 2. The flashlamp output was passed through a 395 nm short pass filter into a 1250 μm diameter light guide. The light guide was coupled to the epi-illuminator of the TE300 microscope, and the output focused on the endothelium using broadband light. For each imaging session, broadband light was used to identify the photolysis region (~70 μm diameter). In this setup, experiments blocking gap junction function using Gap 27 (300 μM) were performed.

Endothelial Ca^{2+} activity induced by cIP_3 photolysis was imaged at a rate of 10 Hz. Baseline Ca^{2+} activity was recorded for 30 s prior to the photolysis of cIP_3. To ensure proper Ca^{2+} store refilling, all cIP_3 uncaging experiments were performed with a minimum of 15 min rest between each photolysis event.

To visualize Ca^{2+} wave propagation, images of active Ca^{2+} wavefronts were created by calculating $\Delta F/F_0$ for each image in the recording. For cIP_3-evoked Ca^{2+} experiments, a maximum intensity projection of the first 5 s (50 frames) immediately following uncaging was taken and presented using either a green or a time-correlated colormap. Propagation area was calculated by applying a Gaussian blur ($\sigma = 10$) to the maximum intensity projections, thresholding the image, and creating a mask from which the area was measured. Since experiments were paired

(unless otherwise stated), images were contrast-matched for control and treatment.

2.7 | Localized Pressure Ejection Experiments

In some experiments, BAPTA/AM (30 μM), U73122 (10 μM) or high K^+ (134 mM, Ca^{2+} free) PSS were focally applied (or "puffed" on) to the blood vessels via pressure ejection from a puffer pipette. In these experiments, a control cIP_3-initiated Ca^{2+} response was first recorded, and the vessels were allowed to reequilibrate for 15 min. For BAPTA/AM and U73122 this was performed in PSS; for high K^+ (Ca^{2+} free) this was performed in Ca^{2+} free PSS to prevent smooth muscle contraction.

The puffer pipette solution contained a pharmacological agent (BAPTA/AM (30 μM) or U73122 (10 μM) or high K^+ (134 mM, Ca^{2+} free) PSS) and a fluorophore (sulforhodamine B, 1 μM) to visualize the region-of-influence of the puffer-ejected solution. After the puffer pipette was positioned ~50 μm from the endothelial surface, directional flow (1.5 mL.min^{-1}) of bath solution was initiated and maintained throughout the experiment to limit the spread of the drugs. In BAPTA/AM and U73122 experiments, the bath solution was PSS; in high K^+ PSS experiments, the bath solution was Ca^{2+}-free PSS.

Pharmacological agents were puffed onto the blood vessels via pressure ejection for a period of time appropriate to the experiment; for BAPTA/AM and U73122 experiments this was 15 min, for high K^+ PSS experiments this was long enough to stabilize flow, ~2 min. Simultaneously, cIP_3-evoked Ca^{2+} activity was imaged in the FITC channel (490 nm excitation) and the sulforhodamine B signal in the TRITC channel (550 nm excitation) at 5 Hz per channel. During the rest period between each experiment, arteries were washed with PSS to replenish internal Ca^{2+} stores.

Puffer pipette locations, bath PSS flow direction, photolysis site, and puffing region are shown and labeled in each image presented. To visualize Ca^{2+} wave propagation, images of active Ca^{2+} wavefronts were created by calculating $\Delta F/F_0$ for each image in the recording. For cIP_3-evoked Ca^{2+} experiments, a maximum intensity projection of the first 5 s (50 frames) immediately following uncaging was taken and presented using either a green or a time-correlated colormap. Propagation area was calculated by applying a Gaussian blur ($\sigma = 10$) to the maximum intensity projections, thresholding the image, and creating a mask from which the area was measured. Since experiments were paired (unless otherwise stated), images were contrast matched for control and treatment.

2.8 | Ca^{2+} Signal Analysis

ACh- or cIP_3-evoked Ca^{2+} signals were measured in each cell as previously described [12]. In brief, automated Fiji macros were used to extract cell coordinates and track cell positions between datasets. Single-cell Ca^{2+} signals were then measured from each cell and processed using a custom algorithm written in the Python programming language [12, 17, 18]. Raw fluorescence (F) signals were converted to baseline-corrected fluorescence intensity (F/F_0) by dividing each intensity measurement by the average value of a 100-frame baseline period at the start of each trace. F/F_0 signals were smoothed using a 21-point third order polynomial Savitzky–Golay filter, and key signal parameters (e.g., amplitude, frequency, number of cells, time of event) were extracted automatically. Analyses of cIP_3-evoked Ca^{2+} responses were performed either within the photolysis region, within the perfusion region, or for the entire field of view (FoV).

To visualize and measure propagation speed, cell coordinates and the time of the first recorded Ca^{2+} peak were extracted. These values were imported into MATLAB R2023b using custom-written code, and the distance versus time plot was generated. A colormap was applied to the time of first activation to produce a color-coded map of coordinates and activation times. The effective speed of signal propagation was calculated by measuring the distance from the uncaging region and the time of first activation.

Analysis of signals in the photolysis region was achieved by applying a mask to the data. The photolysis region was measured from an image acquired during the activation of the flash lamp or laser. For measurements in the region where drugs were applied via pressure ejection, a mask was created using the sulforhodamine signal. Parameters such as the number of active cells within the RoIs, Ca^{2+} response, and propagation area were then extracted.

2.9 | FluoVolt Membrane Potential Experiment

The endothelium was loaded with FluoVolt (1X dye, 10X PowerLoad concentrate, 8 min room temperature) and mounted on imaging system 1.

A bath solution of Ca^{2+}-free PSS was flowed onto the vessel and a control cIP_3 photolysis recording was acquired. The bath solution was changed to PSS for 15 min to refill the Ca^{2+} stores, then the bath solution was changed to Ca^{2+} free PSS. A perfusion pipette solution of High K^+ (134 mM, Ca^{2+} free) PSS with sulforhodamine B (1 μM) was puffed over the photolysis region (as described above) as a second cIP_3 photolysis recording was taken. The bath solution was changed to PSS for 15 min to refill the Ca^{2+} stores, then the bath solution was changed to high K^+ (134 mM, Ca^{2+} free) PSS, and a final cIP_3 photolysis recording was taken.

Images were acquired at 5 Hz per channel, recording the FluoVolt (490 nm excitation) and sulforhodamine (550 nm excitation) channels simultaneously. To acquire traces of the change in fluorescence, regions of interest (indicated in the images shown) were drawn and signals extracted, smoothed using a rolling average of 20, and normalized to the baseline signal.

2.10 | Fluorescent Recovery After Photobleaching (FRAP) Experiments

The endothelium was loaded with calcein/AM (0.02% Pluronic F-127 in PSS) for 30 min at 37°C. FRAP experiments were

performed on imaging system 1 using a ROE DL-Series UV (375 nm) with a UGA-42 scanner (Rapp OptoElectronics). The FRAP region was selected via the controlling software. A 40X 0.8NA water-immersion lens was used in these experiments, and the power was measured at approximately 8 mW. The scan was repeated ~5–10 times in ~5 cells to reduce the fluorescence intensity within the FRAP region to ~70% of the initial value. Images were then acquired at 0.1 Hz for 1 h to image the recovery period.

2.11 | Immunocytochemistry

Freshly isolated endothelial cell patches or *en face* arteries were fixed in 4% paraformaldehyde (PFA; Agar Scientific, UK) in phosphate buffered saline (PBS) (20 min, room temperature), refreshing the PFA after 10 min. Cells were washed (5 min) three times in glycine solution (0.1 M), three times in PBS (5 min), permeabilized with Triton-X100 (0.2% in PBS; 30–45 min), washed three times in PBS (5 min), three times in an antibody wash solution (0.15 M NaCl, 15 mM Na3C6H5O7, 0.05% Triton-X100 in milliQ water; 5 min), and incubated with blocking solution (5% donkey serum in antibody wash solution; 1 h at room temperature). Cells were then incubated overnight at 4°C with an anti-CD31 (PECAM) primary antibody (R&D Systems cat. # AF3628, RRID:AB_2161028, 1:1000, raised in goat), anti-α tubulin (Sigma, Cat # T5168, RRID: AB_477579, 1:1000, raised in mouse) and anti-IP_3R (Millipore, Cat. # 07–1210, RRID:AB_1587207, 1:100, raised in rabbit) primary antibodies, each diluted in antibody buffer at the concentrations stated (0.15 M NaCl, 15 mM Na3C6H5O7, 2% donkey serum, 1% BSA, 0.05% Triton X-100, 0.02% sodium azide in milliQ water). All antibodies were used once. Vessels were washed three times in antibody wash solution (5 min), and incubated with fluorescent secondary antibodies conjugated to the appropriate combination of Alexa Fluor 488 (donkey anti-goat, Cat. # A-11055, RRID:AB_2534102), Alexa Fluor 568 (donkey anti-goat, Cat. # A-11057, RRID: AB_2534104), Alexa Fluor 555 (donkey anti-rabbit, Cat. # A-31572, RRID: AB_162543), Alexa Fluor 647 (donkey anti-rabbit, Cat. # A-31573, RRID: AB_2536183), and Alexa Fluor 488 (donkey anti-mouse, Cat. # A- 21202, RRID: AB_141607) all Invitrogen, 1:1000 dilution, in antibody buffer (1 h at room temperature). Cells were washed three times in antibody wash solution, incubated with the nuclear stain, 4′,6-diamidino-2-phenylindole (DAPI; 4 nM; 5 min), and washed three times in PBS (5 min) prior to imaging. Images were acquired using either a 100X lens on imaging system 2 (endothelial patches) or a 60X 1.0 NA water dipping lens on imaging system 1 (*en face* arterial blood vessels) with 5% LED light (100 ms exposure). 100 images were acquired and averaged for each channel. Images are presented as an average intensity projection with a Gaussian blur ($\sigma = 1$) applied.

2.12 | Solutions and Drugs

Cal520/AM was obtained from Abcam. Pluronic F-127, calcein/AM, FluoVolt Membrane Potential Kit, secondary antibodies: donkey anti-goat 488, donkey anti-goat 568, donkey anti-rabbit 555, donkey-anti rabbit 647, donkey anti-mouse 488 were obtained from Invitrogen. Acetylcholine, NaCl, MOPS, KCl, NaH2PO4, Glucose, EDTA, MgCl, EGTA, U73122, sulforhodamine B, LY294002, wortmannin, Gap27, saponin were obtained from Sigma Aldrich. FR900359 was obtained from Cambridge Bioscience Limited. NF 449, BAPTA/AM, Gallein, YM254890, were obtained from Tocris. Ins(1,4,5) P3-caged IP_3 was obtained from SiChem. All solutions were prepared fresh each day.

2.13 | Data and Statistical Analysis

Summarized data are presented as individual data points, and matched experiments are indicated graphically by lines linking data points; "*n*" refers to the number of animals. Data were compared using various statistical tests, as indicated in the corresponding text and/or figure legends. A post hoc test was only performed if *F* was significant and there was no variance inhomogeneity. All statistical analyses were performed using GraphPad Prism, version 6.0 (GraphPad Software). A p value < 0.05 was accepted as statistically significant. All tests, *n* numbers and significance values are noted in the figure legends.

3 | Results

Endothelial cells line the lumen of arteries and maintain tight cell–cell contact, regulating cell–cell signaling pathways. A dominant form of signaling control for endothelial cells is mediated through IP_3-activated release of Ca^{2+} from internal stores within the endoplasmic reticulum. To explore the mechanisms responsible for intercellular communication, experiments were conducted to visualize propagated Ca^{2+} responses in intact blood vessels. Intracellular Ca^{2+} signaling was initiated by local activation of IP_3Rs in selected cells. This was achieved through the photolysis of a photolabile form of the inositide (caged IP_3; cIP_3). Upon photolysis, cIP_3 triggered a rapid rise in intracellular Ca^{2+} at the activation site, which then propagated radially outwards from the circular uncaging site (Figure 1A). The speed of Ca^{2+} wave was reproducible across experimental repeats (Repeat 1: $73 \pm 7\,\mu m.s^{-1}$, Repeat 2: $70 \pm 13\,\mu m.s^{-1}$; Figure 1A).

Since the propagated response was visualized using the Ca^{2+} indicator, Cal520/AM, we initially hypothesized that Ca^{2+} itself drove the propagation across endothelial cells. To test whether Ca^{2+} was necessary for cIP_3-evoked Ca^{2+} wave propagation, the acetoxymethyl ester (AM) form of the Ca^{2+} chelator, BAPTA, was used to prevent the Ca^{2+} increase from occurring in a selected population of cells to reveal if the Ca^{2+} wave propagated beyond that region. BAPTA/AM was applied continuously for 15 min via a pressure ejection pipette, followed by 15 min for enzymatic hydrolysis of the AM group (Figure 1C). BAPTA/AM was applied to the entire photolysis site and the surrounding cells to ensure that cytoplasmic Ca^{2+} was buffered in all cells where cIP_3 photolysis occurred. The precise region of BAPTA/AM application was visualized using the fluorophore sulforhodamine, which was also present in the puffer pipette. We have previously shown that the application of sulforhodamine onto *en face* blood vessels via pressure ejection does not elicit a Ca^{2+} response [10].

Following BAPTA/AM, photolysis of cIP_3 did not evoke a Ca^{2+} response at the activation site, and there was a significant

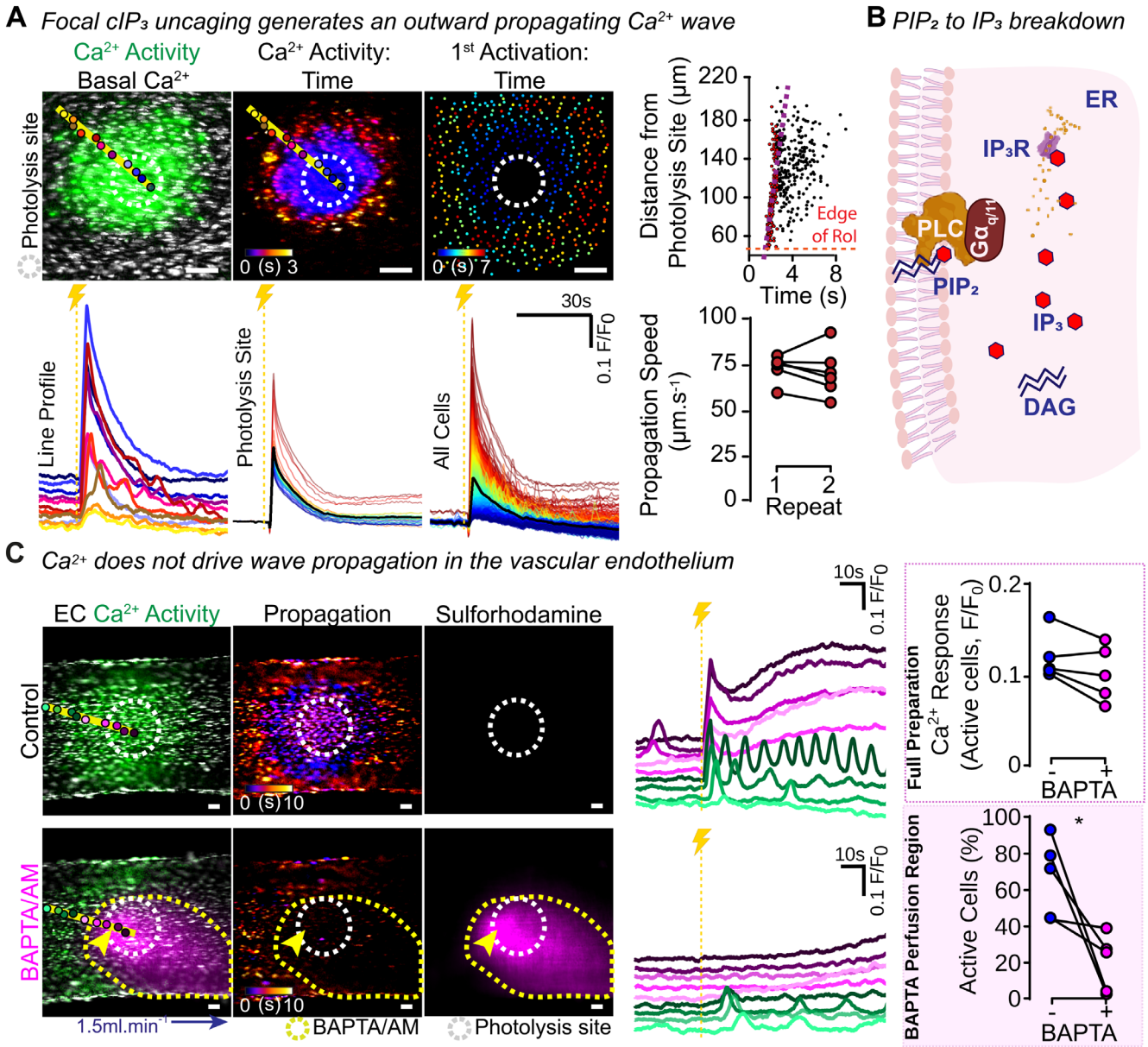

FIGURE 1 | Focal release of caged IP_3 in the vascular endothelium generates an IP_3-dependent radially propagating Ca^{2+} wave. (A) Representative live-cell images of endothelial fields in an *en face* blood vessel loaded with Cal520/AM (5 μM) and cIP_3 (5 μM) show basal Ca^{2+} levels (gray) and cIP_3-evoked Ca^{2+} activity (green). Color-coded time maps of Ca^{2+} propagation for the first 3 s post activation and the first 7 s are shown. Individual traces from cells within the endothelial field are shown using three different methods. Traces are shown from cells underlying the marked circles along the yellow line (line analysis; separated vertically for ease of identification; color corresponding to the identification circles), within the photolysis site, or from every cell in the field (overlaid; color-coded for F/F_0 intensity, from red; high to blue; low). Plotting cell distance from the photolysis site against activation time confirms radial signal propagation. Red points are signals from within the photolysis site. The average Ca^{2+} propagation speed is shown for two repeats, with no significant difference between trials ($p > 0.05$) using a paired Student's *t*-test. (B) Schematic showing activation of phospholipase C (PLC) to mediate breakdown of PIP_2, generate IP_3, and trigger Ca^{2+} release from the endoplasmic reticulum (ER). (C) Endothelial cells loaded with Cal520/AM (5 μM) and cIP_3 (5 μM) show basal Ca^{2+} levels (gray) and cIP_3-evoked Ca^{2+} activity (green) overlaid, color-coded time maps of Ca^{2+} propagation 10 s post uncaging, and the sulforhodamine B signal designating the BAPTA/AM region of influence (magenta), all in the presence of counter-propagating PSS flow (1.5 mL.min^{-1}; blue arrow). Images are shown before and after focal BAPTA/AM (30 μM, 15 min, yellow arrow: Puffer location) application using pressure ejection from a puffer pipette to a preselected endothelial region (yellow dashed line delineating magenta application region). Individual traces from cells within the endothelial field are shown from cells underlying the marked circles along the yellow line (separated vertically for ease of identification; color corresponding to the identification circles). Summary data show that focal buffering of Ca^{2+} with BAPTA/AM does not change the Ca^{2+} response in activated cells across the vessel, but significantly reduces the number of cells activated within the BAPTA/AM puffing region (purple-shaded box, $n = 5$). Yellow dashed line with lightning bolt indicates photolysis. Scale bars = 50 μm. All summary data are matched; *Indicates statistical significance ($p < 0.05$) using a paired Student's *t*-test.

reduction in the number of activated cells within the BAPTA/AM puffing region (Figure 1C). However, outside the Ca^{2+}-buffered region, an outwardly propagating Ca^{2+} response occurred, generating a Ca^{2+} increase equivalent to that seen in the control recording (Figure 1C, Video S1). These findings suggest that an increase in IP_3 is sufficient to drive wave propagation, and that Ca^{2+} itself is not required for signal propagation to occur.

3.1 | Regenerative IP_3 Production Drives Ca^{2+} Wave Propagation

IP_3 generation occurs via activation of phospholipase C (PLC) in the cell membrane, leading to the hydrolysis of phosphatidylinositol-4,5-bisphosphate (PIP_2) to IP_3 (Figure 1B). To investigate whether regenerative IP_3 production was required for endothelial Ca^{2+} wave propagation to occur, we used the PLC inhibitor U73122 (10 μM, 15 min) to focally block PLC activity in a selected population of cells and prevent PIP_2 degradation to IP_3. U73122 was applied locally via pressure ejection in the direction of PSS flow, to a region of cells adjacent to the propagation region, to inhibit PLC (Figure 2A). In the presence of U73122, the propagated Ca^{2+} response was blocked within the U73122-incubated areas, resulting in a significant reduction in the area of propagation (Figure 2A). The number of active cells and the Ca^{2+} response, within the U73122-incubated region, were also significantly decreased (Figure 2A). This finding suggests that regenerative IP_3 production plays a crucial role in Ca^{2+} wave propagation.

To validate the role of regenerative IP_3 production, we inhibited another step in the pathway, PIP_2 generation, using phosphatidylinositol 4-kinase (PI4K) inhibitors LY294002 (300 μM) and wortmannin (50 μM) [19–22]. Incubation of PI4K inhibitors for 30 min significantly reduced the propagation area, restricting it to just beyond the photolysis site, without altering the average cIP_3-evoked Ca^{2+} response in the photolysis site (Figure 2B).

Collectively, these experiments demonstrate that Ca^{2+} does not drive rapid outward wave propagation in mesenteric artery endothelial cells. Instead, regenerative IP_3 production is the key mechanism driving Ca^{2+} wave propagation.

3.2 | IP_3 Diffusion Through Gap Junctions Does Not Influence Ca^{2+} Wave Propagation

The question now arises, what triggers regenerative IP_3 production in cells outside of the photolysis region? A prevalent hypothesis for intercellular Ca^{2+} wave propagation in the endothelium is that gap junctions facilitate movement of IP_3, as a second messenger, operating between cells. Therefore, we next tested the role of gap junctions in wave propagation.

IP_3 is a trivalent anion that is proposed to diffuse passively between cells through gap junctions, driven by the electrochemical gradient operating on the inositide. The increase in IP_3 triggers a rise in intracellular Ca^{2+}, which activates Ca^{2+}-dependent K^+ channels, leading to hyperpolarization of the activated cells. This hyperpolarization will increase the electrochemical gradient for IP_3 movement, thereby facilitating its flux between cells [23]. A further increase in the electrochemical gradient can be achieved by selectively depolarizing those cells that are directly coupled to those releasing IP_3. If gap junctions allow IP_3 passage, as is commonly hypothesized [8, 9], depolarizing adjacent electrically-coupled cells would increase the driving force for IP_3 entry into those cells, promoting more extensive wave propagation.

To test this hypothesis, we depolarized a preselected population of endothelial cells adjacent to the outer edge of the IP_3 photolysis region using high K^+ PSS (134 mM; $E_K \sim -1$ mV), applied focally via a pressure ejection pipette (Figure 3A). These experiments were conducted in Ca^{2+}-free PSS to prevent smooth muscle cell contraction, and the region of high K^+ PSS application was identified using the fluorophore sulforhodamine, which was also present in the puffer pipette.

There was no significant difference between either the F/F_0 responses in cells along the line profile drawn, in the average propagation area within the High K^+-perfused region, or between the active cell number in the High K^+-perfused region (Figure 3A). These results challenge the expectation that gap junctions, by allowing the passive flux of IP_3 between cells, are primarily responsible for mediating wave propagation (Figure 3A, Video S2).

To ensure that membrane potential was depolarized as expected, we first checked that high K^+ PSS blocked cIP_3-evoked hyperpolarization. In these experiments, the endothelium was dual-loaded with the membrane potential indicator FluoVolt and cIP_3. Photolysis of cIP_3 (once again in Ca^{2+}-free PSS) was recorded with either localized high K^+ PSS perfused across the photolysis region or present in the entire bath (Figure 3B). High K^+ PSS in the puffer pipette or throughout the bath each blocked cIP_3-evoked hyperpolarization, as expected from the high K^+-evoked shift in E_K (Figure 3B).

In a separate series of experiments, puffing of high K^+ PSS across the entire vessel did not affect the propagation area, the Ca^{2+} response nor the number of active cells when compared to control responses, evoked in Ca^{2+} free PSS (Figure 3C). This experiment establishes that the store content and responsiveness to IP_3 were unchanged by high K^+ PSS over the time course of the experiments.

As an additional control, to test that each artery used responded appropriately, high K^+ PSS puffed onto the *en face* blood vessels caused a rapid contraction, as expected, when Ca^{2+} was present in the bath PSS (Figure S1).

These results suggest that gap junctions may play a limited role in the movement of IP_3 during Ca^{2+} wave propagation.

The effects of gap junction blockers on wave propagation were also examined in a subsequent series of experiments. While there are many effective pharmacological gap junction blockers, we have previously shown that the widely used inhibitors carbonoxolone and 18β-glycyrrhetinic acid inhibit IP_3R activity and depolarize mitochondria [16], making these inappropriate to use in endothelial Ca^{2+} wave propagation studies. Another

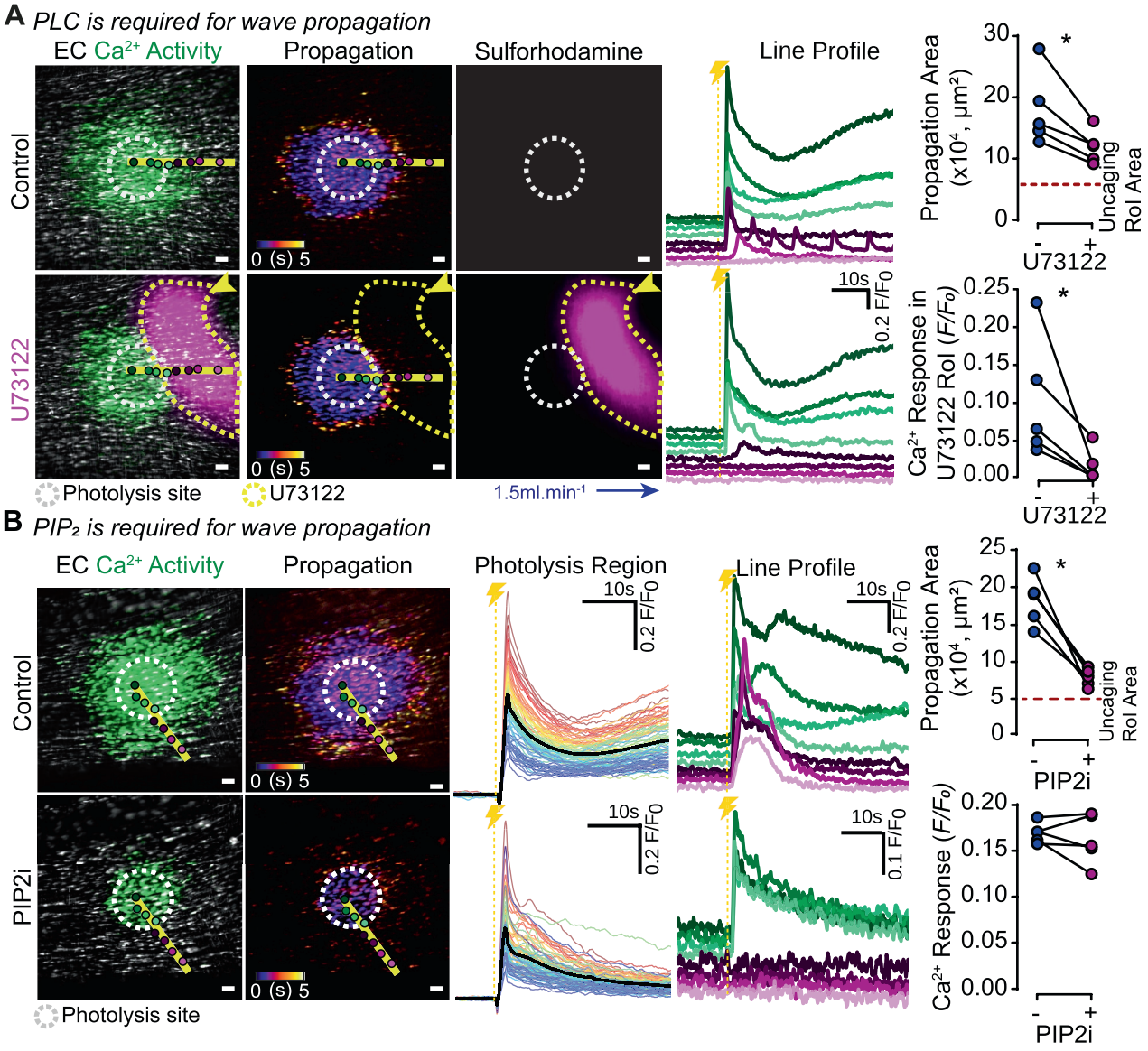

FIGURE 2 | IP_3-mediated IP_3 production, not Ca^{2+}, is required for endothelial Ca^{2+} wave propagation. (A) Representative live-cell images of an endothelial field loaded with Cal520/AM (5 μM) and cIP_3 (5 μM) show basal Ca^{2+} levels (gray) and cIP_3-evoked Ca^{2+} activity (green), color-coded time maps of Ca^{2+} propagation over the first 5 s post activation, and sulforhodamine B (1 μM) signal designating the U73122 region of influence. All images were acquired in the presence of PSS flow (1.5 mL.min^{-1}; blue arrow). Images are shown before and after focal U73122 (10 μM, 15 min, yellow arrow: Puffer location) application using pressure ejection from a puffer pipette to a preselected endothelial region (yellow dashed line delineating magenta application region). Individual traces from cells within the endothelial field are shown from cells underlying the marked circles along the yellow line profile (separated vertically for ease of identification; color corresponding to the identification circles). Summary data show focal PLC inhibition with U73122 significantly reduces the propagation area and the Ca^{2+} response within the region of PLC inhibition ($n = 5$). (B) Representative live-cell images of an endothelial field loaded with Cal520/AM (5 μM) and cIP_3 (5 μM) show basal Ca^{2+} levels (gray) and cIP_3-evoked Ca^{2+} activity (green) and color-coded time maps of Ca^{2+} propagation over the first 5 s post activation. Images are shown before and after global inhibition of PIP_2 synthesis (300 μM LY294002 and 50 μM wortmannin, 30 min). Individual traces from cells within the endothelial field are shown from cells within the photolysis site (overlaid; color-coded for F/F_0 intensity, from red; high to blue; low) or underlying the marked circles along the yellow line profile (separated vertically for ease of identification; color corresponding to the identification circles). Yellow dashed line with lightning bolt indicates photolysis. Summary data show that blocking PIP_2 generation with LY294002 and wortmannin reduces the Ca^{2+} wave propagation area without reducing the average Ca^{2+} response in the photolysis site ($n = 5$). All summary data are matched; *Indicates statistical significance ($p < 0.05$) using a paired Student's *t*-test. Scale bars = 50 μm.

widely used inhibitor, 18α-glycyrrhetinic acid, effectively blocks diffusion through gap junctions, though it does not affect cIP_3-evoked propagation extent [10].

Gap27 is a peptide derived from connexin 43, a connexin subtype that is widely found in the mesenteric vasculature [24], and as such is a selective gap junction blocker [25]. We tested whether

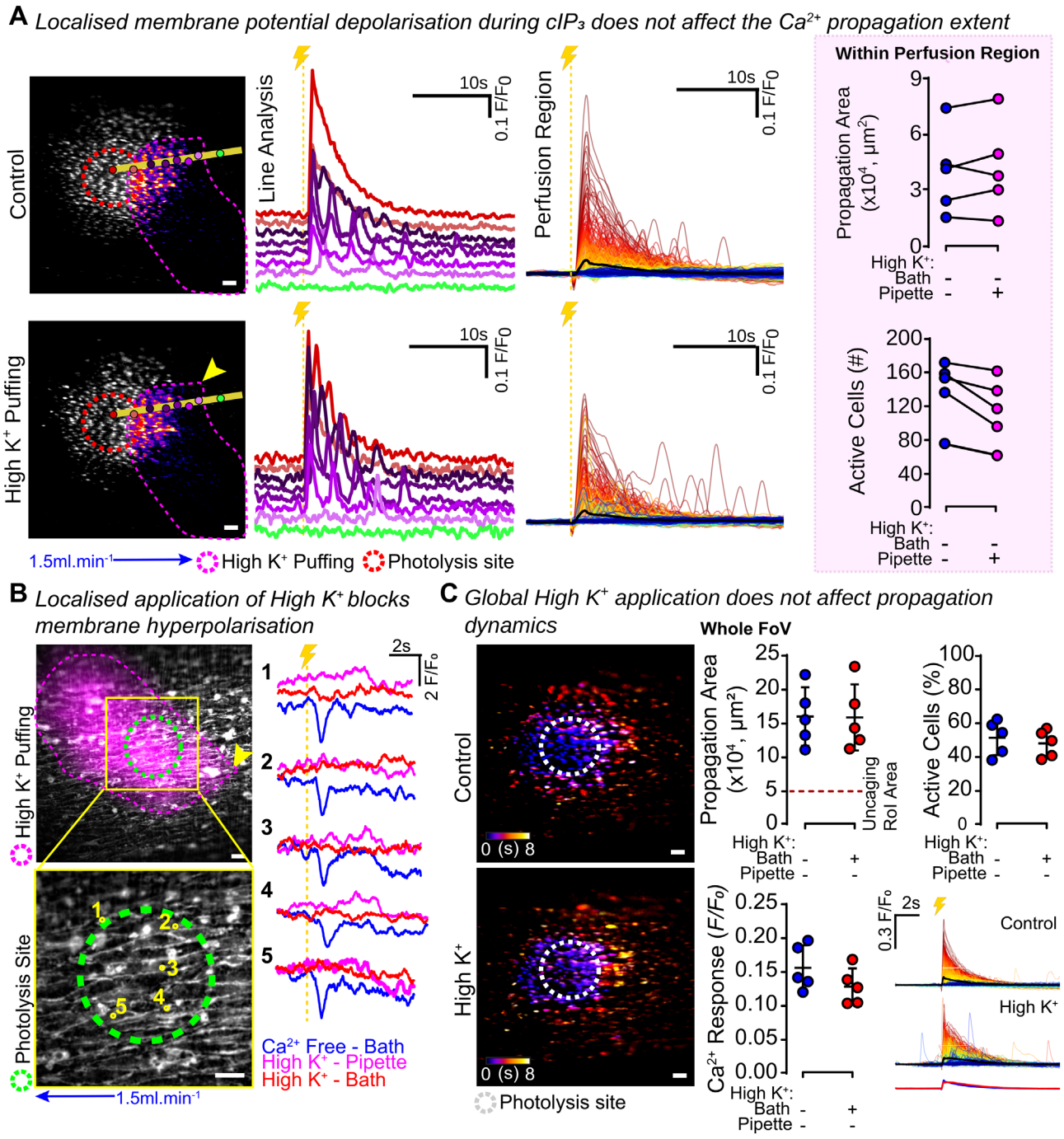

FIGURE 3 | Legend on next page.

or not Gap27 altered wave propagation dynamics in endothelial cells. Gap27 (300µM, 30min) did not alter the average Ca^{2+} response, nor the propagation area of the cIP_3-evoked Ca^{2+} wave (Figure S2A). To verify that gap junctions were being blocked effectively by Gap27 at the concentration and incubation time used, "Fluorescence recovery after photobleaching" (FRAP) experiments were performed in *en face* blood vessels stained with the fluorophore calcein/AM ($MW_{calcein}=620$ Da; $MW_{IP3}=420$ Da). The diffusion of calcein to neighboring cells after photobleaching was recorded. In controls, full recovery occurred after 1h, however this recovery was blocked in the presence of Gap27, suggesting that the blocking of gap junctions occurred (Figure S2B).

This evidence, taken together, suggests that neither gap junctions nor transcellular diffusion plays a role in the rapid, radial IP_3-evoked Ca^{2+} wave propagation.

3.3 | $G\alpha_{q/11}$ GPCRs Are Involved in Regenerative IP_3 Production

The results presented suggest that PLC-mediated regenerative IP_3 production drives wave propagation. It follows that part of an intercell communication bridge may therefore involve IP_3 in one cell, resulting in G protein-mediated activation of PLC in

FIGURE 3 | Localized membrane potential depolarization does not alter Ca^{2+} wave propagation. (A) Representative live-cell images of an endothelial field loaded with Cal520/AM (5 μM) and cIP_3 (5 μM) show cIP_3-evoked Ca^{2+} activity (gray) over the first 5 s postactivation, under control conditions or after focal perfusion of High K^+ (134 mM) PSS using pressure ejection from a puffer pipette to a preselected endothelial region at the outer extent of signal propagation (purple dashed line and FIRE LUT delineating magenta application region; yellow arrow: Puffer location). All images were acquired in the presence of Ca^{2+} free PSS flow (1.5 mL.min^{-1}; blue arrow). Individual traces from cells within the endothelial field are shown from cells within the High K^+ perfusion region (overlaid; color-coded for F/F_0 intensity, from red; high to blue; low) or underlying the marked circles along the yellow line profile (separated vertically for ease of identification; color corresponding to the identification circles). Yellow dashed line with lightning bolt indicated photolysis. Summary data showing that within the High K^+ perfusion region, focal membrane potential depolarization does not change the propagation area, nor the number of active cells ($n = 5$, matched data). (B) Image of an endothelial field stained with FluoVolt (5 min incubation, gray). Signal traces are shown from 5 locations (numbered yellow labels) under control conditions (counter propagating Ca^{2+} free PSS; blue line), high K^+ PSS puffed onto the vessel using pressure ejection from a puffer pipette in the presence of counter propagating Ca^{2+} free PSS (magenta application region; magenta line), and global counter propagating high K^+ PSS (red line) in the entire bath. (C) Color-coded time maps of cIP_3-evoked Ca^{2+} propagation over the first 5 s postactivation under control conditions (Ca^{2+} free PSS) or after global high K^+ (134 mM) PSS. Summary data show that high K^+ (134 mM) PSS does not affect the propagation area, the Ca^{2+} response nor the number of cells activated ($n = 5$). Representative traces of Ca^{2+} activity from each cell within the field of view are shown; the average signal is represented by a thick line and shown overlaid. Perfusion region-of-influence was determined using sulforhodamine B (1 μM) signal. *Indicates statistical significance ($p < 0.05$) using a paired Student's *t*-test. All High K^+ PSS is also Ca^{2+}-free to avoid contraction of arteries. Scale bars = 50 μm.

a neighbor to evoke the breakdown of PIP_2 into IP_3 in the cells outside the photolysis site.

To test this possibility, a selective inhibitor of $G\alpha_q$-mediated signaling (YM254890; 1 μM, 30 min) [26] was first used. YM254890 blocked propagation of cIP_3-evoked Ca^{2+} waves, significantly reducing the number of active cells while having no effect on the cIP_3-evoked Ca^{2+} response within the photolysis region (Figure 4Ai, Video S3).

$G\alpha_{q/11}$ GPCRs are activated by the M3 muscarinic receptor; therefore, confirmation of YM254890 inhibitory activity was achieved using the M3 agonist ACh. ACh controls, performed in the same arterial blood vessels, were blocked when $G\alpha_{q/11}$ GPCR activity was inhibited by YM254890, causing a significant decrease in both the average Ca^{2+} response and the percentage of ACh-activated cells (Figure 4Aii). These results suggest that $G\alpha_{q/11}$ contributes to Ca^{2+} wave propagation.

A second $G\alpha_{q/11}$ inhibitor (FR900359; 5 μM, 30 min) [27] was used to confirm these findings. The extent of cIP_3-evoked propagation and the number of active cells were significantly decreased in the presence of FR900359 while the cIP_3-evoked Ca^{2+} increase in the photolysis site was unaltered (Figure 4Bi). The ACh-evoked Ca^{2+} response and the number of activated cells by ACh were significantly decreased by FR900359, confirming the inhibition of $G\alpha_q$ G proteins. Taken together, these data (Figure 4Bii) suggest a novel role for $G\alpha_{q/11}$ GPCRs as part of the transcellular communication bridge, facilitating regenerative IP_3 production in wave propagation.

3.4 | $G_{i/o}$, G_s and Gβγ GPCRs Are Not Involved in Regenerative IP_3 Production

PLCβ exists in four distinct isoforms (1–4), which have each been shown to respond to stimuli from either $G\alpha_q$ GPCRs or G_i- and Gβγ-GPCRs (from G_i-Gβγ heterodimers) [28]. G_i or Gβγ subunits may also contribute to the regenerative IP_3 production pathway via activation of distinct PLC isoforms. To test this, we inhibited the signaling of the Gβγ and $G_{i/o}$ subunits.

The Gβγ subunit signaling inhibitor, Gallein (5 μM, 30 min) [29] failed to alter the cIP_3-evoked propagation area or Ca^{2+} response (Figure 5Ai). Similarly, the $G_{i/o}$ inhibitor pertussis toxin (PTX, 100 ng.ml^{-1}, 4 h) [30] did not alter the cIP_3-activated Ca^{2+} response, nor the cIP_3-evoked propagation area (Figure 5Aii).

G_s proteins primarily act to increase cAMP levels within cells via stimulation of adenylyl cyclases [31]. Some studies have also shown that agonist binding to $G\alpha_s$ stimulates PLC activity [32]. However, the G_s inhibitor NF 449 (1 μM, 30 min) [33] did not affect the cIP_3-evoked Ca^{2+} response, or the propagation area of the outwardly propagating wave (Figure 5Aiii).

Interestingly, whilst no changes were seen in the number of ACh-activated cells in the presence of these Gβγ, $G_{i/o}$, or G_s inhibitors, there was a consistent *increase* in ACh-elicited Ca^{2+} responses in the presence of gallein and NF499 (Figure 5Bi–iii).

These results suggest that Gβγ, $G_{i/o}$, and G_s G protein subfamilies do not play a role in the IP_3-evoked IP_3 regenerative signaling cascade.

3.5 | IP_3 Receptors Are Located at the Plasma Membrane of Endothelial Cells

Collectively, the results thus far show that regenerative IP_3 production, rather than Ca^{2+} itself, drives the propagation of Ca^{2+} waves, facilitated by transcellular activation of a $G\alpha_{q/11}$-coupled GPCR. These findings raise the question of how regenerative IP_3 signaling is initiated and transmitted between neighboring cells during wave propagation?

A potential explanation is the presence of IP_3Rs at the plasma membrane, which could act as transmembrane signaling hubs. These IP_3Rs could activate a $G\alpha_{q/11}$-coupled GPCR on the adjacent receiving cell (without requiring ion permeation), triggering PLC-mediated hydrolysis of PIP_2 into IP_3 and propagating the signal to neighboring cells.

To determine whether IP_3Rs are found at or near the plasma membrane, endothelial cell patches were simultaneously stained

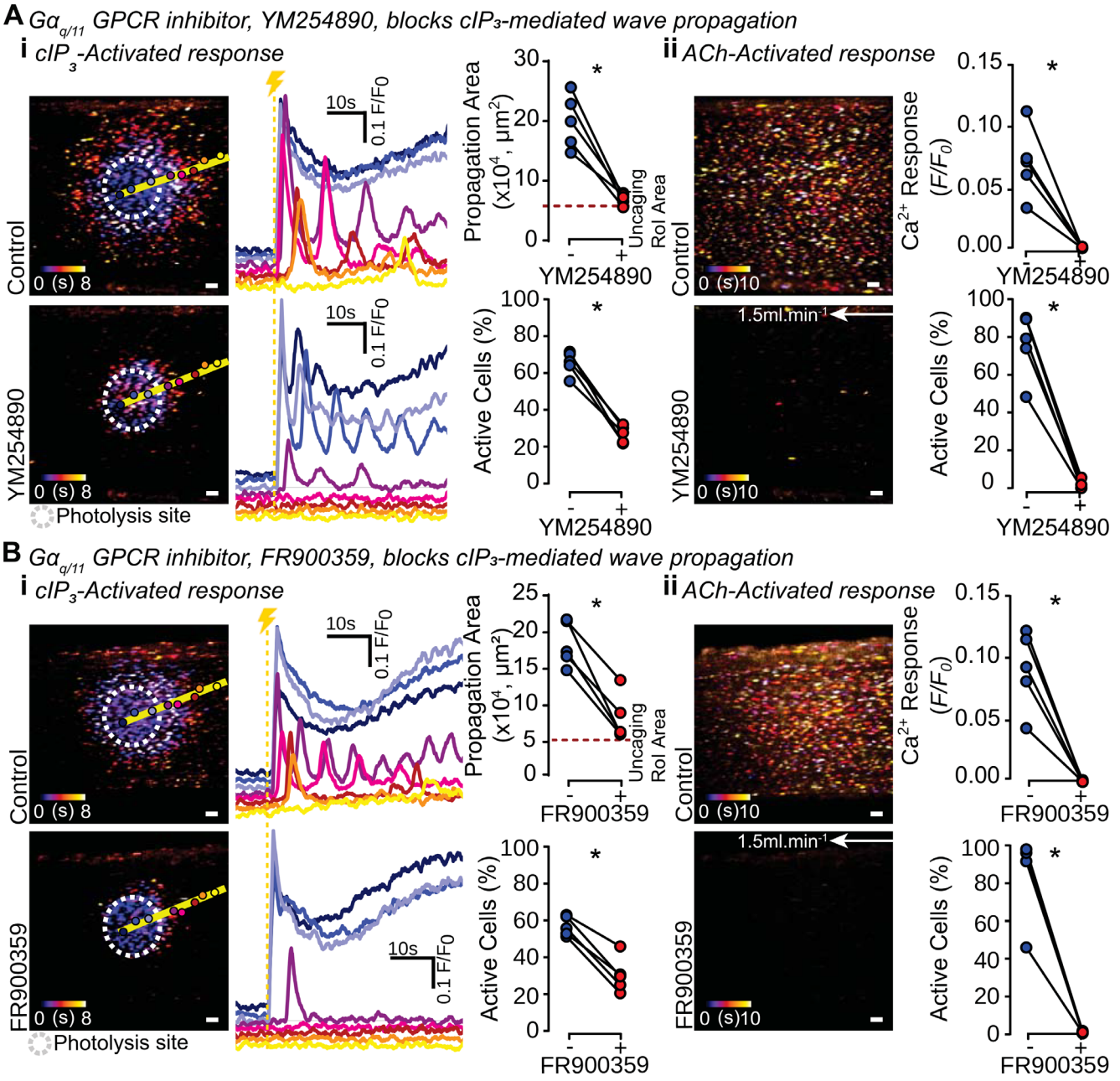

FIGURE 4 | Gα$_{q/11}$ GPCRs are required for regenerative IP$_3$-mediated IP$_3$ production. Representative live-cell images of an endothelial field loaded with Cal520/AM (5 µM) and cIP$_3$ (5 µM) show basal Ca^{2+} levels (gray) and color-coded time maps of Ca^{2+} propagation arising from (i) cIP$_3$-generated and (ii) ACh (100 nM)-generated activation. Images are shown under control conditions or after Gα$_{q/11}$ inhibition across the entire vessel using (A) YM254890 (1 µM, 30 min) or (B) FR900359 (5 µM, 30 min). Individual traces from cells within the endothelial field are shown from cells underlying the marked circles along the yellow line profile (separated vertically for ease of identification; color corresponding to the identification circles). A yellow dashed line with a lightning bolt indicates photolysis. Summary data show that blocking Gα$_{q/11}$ GPCR activity with either YM254890 or FR900359 reduces the cIP$_3$-evoked propagation area and number of activated cells ($n = 5$). A significant decrease in the number of ACh-evoked activated cells and the Ca^{2+} response in YM254890-incubated or FR900359-incubated vessels ($n = 5$) was seen. Summary data are all matched; *Indicates statistical significance ($p < 0.05$) using a paired Student's *t*-test. Scale bars = 50 µm.

using an anti-PECAM (platelet endothelial cell adhesion molecule; CD31) antibody to label the plasma membrane, and an anti-IP3R1 antibody to label IP$_3$Rs (Figure 6). The results show that although IP$_3$R distribution is primarily concentrated within the endothelial cell body, there is a peripheral, near-membrane localization of IP$_3$R clusters (arrowheads, Figure 6A). Using data from endothelial cell patches ($n = 6$ patches), an average of 17 ± 4 IP$_3$R clusters per cell colocalized with CD31 staining (Figure 6B).

4 | Discussion

In this study we show that elevated levels of IP$_3$ in endothelial cells trigger a noncanonical inside-out signaling mechanism to transcellularly activate Gα$_{q/11}$-coupled receptors in neighboring cells. Outside-in GPCR activation then triggers canonical PLC-mediated hydrolysis of PIP$_2$ into IP$_3$. This inside-out outside-in signaling mechanism drives a regenerative, IP$_3$-dependent

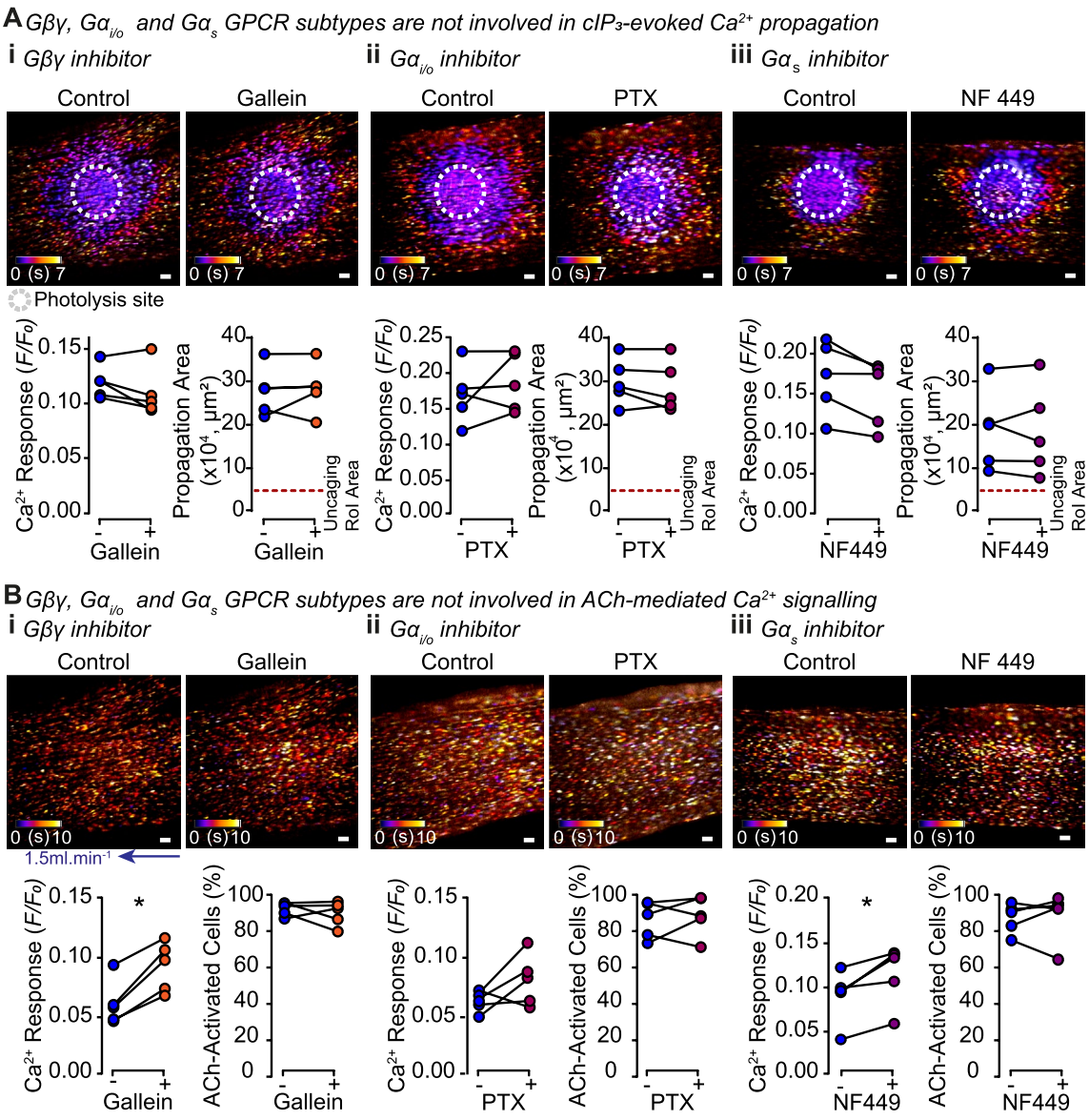

FIGURE 5 | Gβγ, Gα$_{i/o}$, and Gα$_s$ GPCRs are not involved in regenerative IP$_3$-mediated IP$_3$ production. Representative live-cell images of an endothelial field loaded with Cal520/AM (5 µM) and cIP$_3$ (5 µM) show color-coded time maps of (A) cIP$_3$-evoked or (B) ACh-evoked Ca^{2+} propagation, under control conditions and after global (i) Gβγ inhibition using Gallein (5 µM, 30 min), (ii) Gα$_{i/o}$ inhibition using Pretussis toxin (PTX 100 ng.mL^{-1}, 4 h), or (iii) Gα$_s$ inhibition using NF 449 (1 µM, 30 min). Summary data show that blocking Gβγ, Gα$_{i/o}$, or Gα$_s$ GPCR activity with either Gallein, PTX, or NF 449, respectively, does not alter the cIP$_3$-activated Ca^{2+} response, nor does it reduce the propagation area ($n = 5$). In ACh controls, summary data show no alteration in the number of cells activated, and an increase in the ACh-activated Ca^{2+} response ($n = 5$). Summary data are all matched; *Indicates statistical significance ($p < 0.05$) using a paired Student's *t*-test. Scale bars = 50 µm.

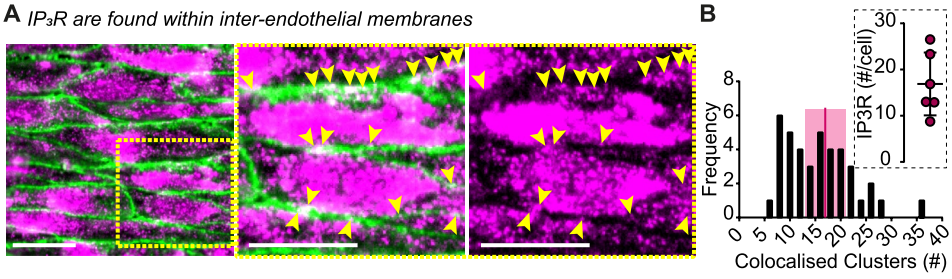

FIGURE 6 | IP$_3$R clusters are located near interendothelial membranes. (A) Immunofluorescence imaging of *en face* preparations with endothelial cells labeled for CD31/PECAM (green) and IP$_3$Rs (magenta) shows colocalization (white) of IP$_3$Rs with PECAM-positive cell membrane regions. (B) Images were analyzed to count IP$_3$R clusters located at the membrane (yellow arrowheads). A histogram displays the distribution of IP$_3$R clusters counted across six endothelial cell patches, with the average cluster count overlaid. Scale bars = 20 µm.

signaling cascade between adjacent cells, facilitating intercellular communication. Importantly, the diffusion of Ca^{2+} or IP_3 through gap junctions does not contribute significantly to this process.

In the endothelium, intercellular communication, over various time and spatial scales, is essential for coordinating physiological adjustments. Intercellular communication ensures precise, timely, and synchronized regulation of critical processes, such as vessel tone modulation, alterations in vascular permeability, and the regulation of immune responses.

Ca^{2+} is a key second messenger that acts both as a trigger for functional responses and as a potential mediator of intercellular signal transmission. However, understanding the specific role of Ca^{2+} and the precise mechanisms driving intercellular signal propagation within the endothelium remains a significant challenge. In the endothelium, the major source of Ca^{2+} in agonist activation is the release of the ion from the internal stores via the PLCβ-PIP_2-IP_3 pathway. PLCβ is the major G protein-coupled enzyme that facilitates the breakdown of PIP_2 into IP_3 and DAG, leading to IP_3-IP_3R binding at the ER and the release of Ca^{2+} into the cytoplasm. In this study, we induced the release of Ca^{2+} from internal stores in an IP_3-dependent, but PLC-independent, manner. We then used pharmacological interventions to target each step of the PLC/Ca^{2+} signaling pathway to determine the mechanisms responsible for the propagation of intercellular cIP_3-evoked Ca^{2+} waves. The results demonstrate regenerative IP_3-mediated IP_3 production, rather than the Ca^{2+} ion itself, drives Ca^{2+} wave propagation.

Two main lines of evidence support this conclusion. First, the Ca^{2+} chelator BAPTA/AM, selectively applied around the uncaging region, prevented Ca^{2+} from increasing after the local release of IP_3. However, after the release of IP_3, a Ca^{2+} wave propagated outside the BAPTA-buffered region even though no IP_3 had been released at these sites. These data show that IP_3 generates a propagating Ca^{2+} wave but that the Ca^{2+} ion itself is not required for waves to propagate (Figure 1C). There was a slight reduction in the amplitude of the Ca^{2+} response in the presence of BAPTA/AM compared to the corresponding signal in the paired control, which could be attributed to low levels of BAPTA/AM diffusing beyond the perfusion area, leading to partial intracellular buffering. This finding is consistent with our previous work, which demonstrated that, although the photolabile Ca^{2+} chelator Diazo-2/AM effectively blocked a cIP_3-induced Ca^{2+} increase at the photolysis site, a Ca^{2+} wave still propagated radially beyond the photolysis site [10].

Secondly, we show the cIP_3-evoked Ca^{2+} wave failed to propagate into regions where PLC had been selectively inhibited (Figure 2A) or where PI4K inhibitors [20] had been used to prevent the PIP_2 hydrolysis necessary for IP_3 production (Figure 2B). These results demonstrate that an IP_3-dependent mechanism activates PLC, leading to the production of IP_3 in adjacent cells, thereby facilitating the propagation of regenerative Ca^{2+} waves. This process is independent of the rise in Ca^{2+}.

Next, we sought to determine the nature of the link between an increase in IP_3 and PLC activation. PLCβ activation and subsequent breakdown of PIP_2 into IP_3 is a process often initiated by GPCRs on the outer plasma membrane [34], therefore we hypothesized that a transcellular form of G protein signaling plays a role in this intercellular communication pathway.

GPCRs are membrane-spanning receptors that customarily act as an interface between agonist-binding at the cell surface and the resulting cascade of intracellular signaling that affects cell function. G proteins are heterotrimeric structures that contain three distinct subunits: membrane-bound α and γ subunits, and β subunits that exist as a dimer with γ. In the inactive state, GDP is bound to the Gα subunit. Agonist-binding causes a conformational change in the GPCR, releasing GDP from Gα and allowing GTP to bind, releasing the Gα-GTP and Gβγ subunits to effect downstream signaling [35].

There are four prominent classes of G protein families: $G\alpha_{q/11}$, $G\alpha_{i/o}$, $G\alpha_s$ and Gβγ. Since $G\alpha_{q/11}$ is the primary G protein subfamily that activates PLCβ at the plasma membrane [2, 3], it was tempting to speculate that it may be involved in regenerative IP_3-mediated wave propagation. Using the $G\alpha_{q/11}$ inhibitors YM254890 and FR900359, we show for the first time that regenerative IP_3-mediated Ca^{2+} wave propagation is dependent on transcellular $G\alpha_{q/11}$ signaling. YM254890 [26, 36] and FR900359 [27, 37] each block the exchange of GDP for GTP during $G\alpha_{q/11}$ activation by binding the cleft between two interdomain linkers connecting the $G\alpha_q$ GTPase and helical domains required for nucleotide access to the binding site. Previous studies found no off-target $G\alpha_i$–coupled receptor activity of YM254890, nor any indication that PLCβ and its downstream signaling pathway were targeted [38]. Effective inhibition of $G\alpha_{q/11}$-mediated activity via both drugs was confirmed by successful inhibition of ACh-mediated M3-receptor $G\alpha_{q/11}$ activation (Figure 4). Furthermore, FR900359 $G\alpha_{q/11}$ inhibition has also been confirmed by reversing phenylephrine-mediated α1-adrenergic receptor–dependent constriction of tail arteries [37]. Neither YM254890 nor FR900359 affected the amplitude of the IP_3-evoked Ca^{2+} response when the receptor was directly activated by IP_3, indicating that the inhibitors did not have any off-target binding downstream of the membrane GPCR signaling. Since the G protein inhibitors (YM254890 and FR900359) prevent wave propagation evoked by direct activation of IP_3R, we show for the first time that $G\alpha_{q/11}$ release and activation of PLC are required for intercellular signal propagation to occur. Our results also suggest that none of $G\alpha_{i/o}$, $G\alpha_s$ or Gβγ contributes to IP_3-mediated Ca^{2+} wave propagation.

Whilst the present experiments provide a key insight into the signaling pathway, they do not elucidate the whole picture. Our results show that IP_3 produced in one cell can trigger IP_3 and Ca^{2+} release in neighboring cells, leading to the propagation of Ca^{2+} waves across the endothelium. This process therefore relies on both inside-out and outside-in signaling. While the precise mechanisms are unclear, our findings suggest that IP_3 activates an IP_3 receptor at the plasma membrane of the initiating cell (inside-out signaling), which then directly or indirectly engages a $G\alpha_{q/11}$-linked GPCR on an adjacent cell. This GPCR activation initiates outside-in signaling, resulting in further IP_3 production from PLC-PIP_2 and continuing the propagation cycle. A membrane-spanning unit on the initiating cell must exist to activate the $G\alpha_{q/11}$-coupled receptor on the receiving cell. This proposal is summarized in Figure 7,

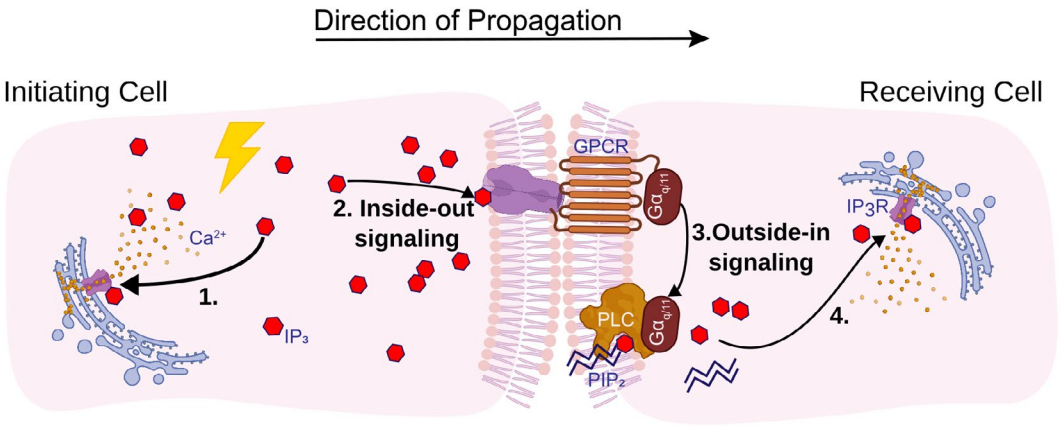

FIGURE 7 | Summary of the proposed IP_3-mediated signaling pathway that maintains intercellular communication in the vascular endothelium. (1) IP_3 activates IP_3R on the endoplasmic reticulum within the initiating cell, releasing Ca^{2+} into the cytoplasm. (2) The signal is passed through to the receiving cell via a transmembrane signaling unit, in a process of "Inside-out signaling." Since IP_3 is required for signal transmission, we hypothesize that this is mediated by pore dead IP_3Rs, clustered at the membrane. (3) This inside-out signal activates a GPCR on the receiving cell membrane, in an "Outside-in signaling" process, releasing the $G\alpha_{q/11}$ subunit to bind to PLC, allowing it to mediate the breakdown of PIP_2 into free IP_3 and DAG in the receiving cell cytoplasm. This is regenerative IP_3 production. (4) Newly-generated IP_3 then binds the IP_3R on the ER in the receiving cells, releasing Ca^{2+} and starting the regenerative process over again to propagate the signal along the vascular endothelium.

where an increase in IP_3 in the initiating cell causes Ca^{2+} release from the internal stores (1). IP_3 then triggers an event on the initiating cell plasma membrane (2) which leads to the activation of a $G\alpha_{q/11}$-coupled receptor on the receiving cell membrane (3). The $G\alpha_{q/11}$ subunit is released, activating PLC-mediated breakdown of PIP_2 into IP_3 and DAG, with IP_3 binding to IP_3R and releasing Ca^{2+} into the cytoplasm of the receiving cell (4). However, a critical question remains: how are signals transmitted between adjacent cells?

One possibility is via gap junctions. Gap junctions consist of linked connexin hemichannels on adjacent cell boundaries which connect the cytoplasm of each cell via a transmembrane pore [39]. Gap junctions have been proposed to play a role in intercellular communication in many cell types [40–43], including the vascular endothelium [44–47]. It has been widely reported that endothelial Ca^{2+} wave propagation is facilitated by diffusion of IP_3 through gap junctions, causing an increase in intracellular Ca^{2+} by binding to IP_3Rs and initiating further Ca^{2+}-induced IP_3 production [5, 9, 48]. While we also clearly see diffusion through gap junctions (Figure S2 [10]), the time scale required for this signal propagation to occur does not align with the speed of cIP_3-evoked radial propagation. Photolysis of 5 μM of caged IP_3 generates 0.5 μM IP_3, which is hydrolyzed at ~0.3 $\mu M.s^{-1}$. IP_3 itself has a short half-time (~1 s) [49] and a predicted range of action of 14 μm [50]. On the other hand, the measured propagated Ca^{2+} waves last for tens of seconds and extend hundreds of microns. This evidence suggests that diffusion of IP_3 itself is unlikely to account for wave propagation.

Further evidence that challenges the involvement of IP_3 diffusion between cells is provided by the observation that changes in the plasma transmembrane potentials do not affect Ca^{2+} wave propagation. IP_3 is a trivalent anion, and any flux between cells via gap junctions will be influenced by the electrochemical driving force acting on the inositide. Following a localized increase in IP_3, depolarization of neighboring electrically coupled cells will enhance the electrochemical driving force for IP_3 flux between cells. This depolarization should thereby promote more extensive wave propagation. However, no increase in wave propagation was observed. In these experiments, a high K^+ (Ca^{2+} free) PSS was applied to cells adjacent to the photolysis site in which IP_3 was released (Figure 3). The high K^+ PSS will produce around a 40 mV depolarization and clamp the membrane potential to ~−1 mV. This membrane potential change is equivalent, in terms of the change in driving force acting on IP_3, to a 125-fold increase in the concentration of IP_3 in the activated cells. Despite the increased driving force, no change in wave propagation occurred. These experiments suggest that diffusion of uncaged IP_3 between cells via gap junctions is unlikely to drive wave propagation.

The role of gap junctions in permitting diffusion of second messengers is often examined using pharmacological inhibitors. However, many of these inhibitors have off-target effects, so they must be used with caution when investigating intercellular Ca^{2+} wave propagation. 18β-glycyrrhetinic acid and carbenoxolone block IP_3R activity [16], and alcohol-based blockers such as octanol and heptanol similarly dampen IP_3-mediated Ca^{2+} release and capacitative Ca^{2+} entry [51]. These effects of the inhibitors will block intercellular Ca^{2+} propagation independently of the contribution of gap junctions to the process. Attention should therefore be given to ensuring an unaltered initial Ca^{2+} response when interpreting the reduction of intercellular Ca^{2+} waves by gap junction inhibitors.

In the present study, we show that Gap27, a specific connexin 43 mimic that blocks gap junction function [52], inhibits fluorophore diffusion after FRAP (a positive control) but does not affect cIP_3-evoked Ca^{2+} wave propagation. Previously, we showed that the broad spectrum gap junction blocker 18α-glycyrrhetinic acid effectively blocked diffusion between endothelial cells but did not affect wave propagation [10]. Neither drug altered the cIP_3-evoked Ca^{2+} response within the photolysis region. Given that neither gap junctions nor diffusion appears to be involved, the question now arises: How are signals transmitted across the membranes from the initiating to the receiving cell?

The data presented suggests that IP_3 is required to drive the propagating Ca^{2+} wave; therefore, IP_3 must trigger signal propagation across the membrane, either directly or indirectly. Our results show that whilst IP_3Rs are predominantly found throughout the cytoplasm, there is a peripheral, near-membrane localization of IP_3R clusters (Figure 6). This interpretation is consistent with previous studies reporting peripheral IP_3R localization [53–55], as well as with the functional data presented in this manuscript. IP_3R are now appreciated to support functions that are completely separate from the Ca^{2+} release activity of the channel. The functions documented thus far include triggering Ca^{2+} influx in staurosporine-induced cell death [56], facilitating interactions of active STIM1 and Orai to promote store-operated Ca^{2+} entry [53, 57] and providing structural roles in linking the endoplasmic reticulum and mitochondria [58]. Flux of Ca^{2+} through IP_3R is not required to support each of these functions. Several other ionotropic receptors that previously have been thought to mediate their physiological effects *only* via the permeation of ions are now known to have important signaling features that do not arise from their ion flux capabilities. AMPA glutamate receptors and N-methyl D-aspartate receptors [59], the kainate receptor [60], the nicotinic acetylcholine receptor [61], the Kv1.3 potassium channel [62] and voltage-dependent Ca^{2+} channels [63] all have signaling functions that are independent of ion flux through the channel pore. For example, activation of the ionotropic glutamate kainate receptor by the neurotransmitter gamma-aminobutyric acid involves activation of PLC and protein kinase C via a Pertussis toxin–sensitive G protein rather than ion flux through the channel [60]. These studies highlight a diversity of signaling pathways that are activated and mediated by functionalities completely unrelated to the channels' ion carrying capabilities. It is therefore tempting to speculate that a receptor for IP_3, which does not conduct ions, anchored at the interendothelial membrane, serves as the key link for propagating the signal to neighboring cells.

Rapid, accurate endothelial cell communication is fundamental to maintaining normal vascular function by transmitting information to dynamically regulate blood flow, mediate changes in vessel permeability, and to control immune responses. In the present study, the use of an *en face* blood vessels coupled with highly localized photolysis of caged IP_3 and rapid, high-resolution image acquisition permitted precise control of the time and location of IP_3R activation within the intact endothelium. Each signal recorded outside the photolysis region arises as a direct consequence of the intercellular signaling cascade triggered by released IP_3. Our results demonstrate a novel role for $G\alpha_{q/11}$ subunit-coupled GPCRs in mediating the propagation of Ca^{2+} waves within the endothelium. Importantly, our findings confirm that regenerative IP_3 production, rather than Ca^{2+} itself, serves as the primary mechanism by which endothelial cells convey intercellular signals.

Author Contributions

C.B., J.G.M.: conceptualization. C.B., C.W., M.D.L., X.Z., J.G.M.: methodology. C.B., J.G.M.: investigation. C.B., J.G.M.: writing – original draft. C.B., M.D.L., C.W., X.Z., J.G.M.: writing – review and editing. J.G.M., C.W., M.D.L., X.Z., C.B: funding acquisition.

Acknowledgments

This work was funded by the British Heart Foundation (RG/F/20/110007), whose support is gratefully acknowledged. The authors would like to thank Margaret MacDonald for her excellent technical support.

Conflicts of Interest

The authors declare no conflicts of interest.

Data Availability Statement

All study data are included in the article and Supporting Information.

References

1. M. D. Lee, C. Buckley, X. Zhang, et al., "Small-World Connectivity Dictates Collective Endothelial Cell Signaling," *Proceedings of the National Academy of Sciences* 119 (2022): e2118927119.

2. S. J. Taylor, H. Z. Chae, S. G. Rhee, and J. H. Exton, "Activation of the β1 Isozyme of Phospholipase C by α Subunits of the Gq Class of G Proteins," *Nature* 350 (1991): 516–518.

3. C. H. Lee, D. Park, D. Wu, S. G. Rhee, and M. I. Simon, "Members of the Gq Alpha Subunit Gene Family Activate Phospholipase C Beta Isozymes," *Journal of Biological Chemistry* 267 (1992): 16044–16047.

4. B. E. Isakson, S. I. Ramos, and B. R. Duling, "Ca2+ and Inositol 1,4,5-Trisphosphate-Mediated Signaling Across the Myoendothelial Junction," *Circulation Research* 100 (2007): 246–254.

5. L. Leybaert and M. J. Sanderson, "Intercellular Ca2+ Waves: Mechanisms and Function," *Physiological Reviews* 92 (2012): 1359–1392.

6. J. C. Sáez, J. A. Connor, D. C. Spray, and M. V. Bennett, "Hepatocyte Gap Junctions Are Permeable to the Second Messenger, Inositol 1,4,5-Trisphosphate, and to Calcium Ions," *Proceedings of the National Academy of Sciences* 86 (1989): 2708–2712.

7. V. H. Hernandez, M. Bortolozzi, V. Pertegato, et al., "Unitary Permeability of Gap Junction Channels to Second Messengers Measured by FRET Microscopy," *Nature Methods* 4 (2007): 353–358.

8. A. G. Wolpe, C. A. Ruddiman, P. J. Hall, and B. E. Isakson, "Polarized Proteins in Endothelium and Their Contribution to Function," *Journal of Vascular Research* 58 (2021): 65–91.

9. A. P. Thomas, G. S. Bird, G. Hajnóczky, L. D. Robb-Gaspers, and J. W. Putney, "Spatial and Temporal Aspects of Cellular Calcium Signaling," *FASEB Journal* 10 (1996): 1505–1517.

10. C. Buckley, M. D. Lee, X. Zhang, C. Wilson, and J. G. McCarron, "Signalling Switches Maintain Intercellular Communication in the Vascular Endothelium," *British Journal of Pharmacology* 181 (2024): 2810–2832.

11. N. Percie du Sert, V. Hurst, A. Ahluwalia, et al., "The ARRIVE Guidelines 2.0: Updated Guidelines for Reporting Animal Research," *Experimental Physiology* 105 (2020): 1459–1466.

12. C. Wilson, M. D. Lee, and J. G. McCarron, "Acetylcholine Released by Endothelial Cells Facilitates Flow-Mediated Dilatation: Autocrine/Paracrine Action of Endothelial ACh," *Journal of Physiology* 594 (2016): 7267–7307.

13. A. D. Edelstein, M. A. Tsuchida, N. Amodaj, H. Pinkard, R. D. Vale, and N. Stuurman, "Advanced Methods of Microscope Control Using μManager Software," *Journal of Biological Methods* 1 (2014): e10.

14. A. Edelstein, N. Amodaj, K. Hoover, R. Vale, and N. Stuurman, "Computer Control of Microscopes Using μManager," *Current Protocols in Molecular Biology* 92 (2010): 14–20.

15. C. Buckley, C. Wilson, and J. G. McCarron, "FK506 Regulates Ca^{2+} Release Evoked by Inositol 1,4,5-Trisphosphate Independently of

FK-Binding Protein in Endothelial Cells," *British Journal of Pharmacology* 177 (2020): 1131–1149.

16. C. Buckley, X. Zhang, C. Wilson, and J. G. McCarron, "Carbenoxolone and 18β-Glycyrrhetinic Acid Inhibit Inositol 1,4,5-Trisphosphate-Mediated Endothelial Cell Calcium Signalling and Depolarise Mitochondria," *British Journal of Pharmacology* 178 (2021): 896–912.

17. C. Wilson, C. D. Saunter, J. M. Girkin, and J. G. McCarron, "Advancing Age Decreases Pressure-Sensitive Modulation of Calcium Signaling in the Endothelium of Intact and Pressurized Arteries," *Journal of Vascular Research* 53 (2016): 358–369.

18. C. Wilson, C. D. Saunter, J. M. Girkin, and J. G. McCarron, "Clusters of Specialized Detector Cells Provide Sensitive and High Fidelity Receptor Signaling in the Intact Endothelium," *FASEB Journal* 30 (2016): 2000–2013.

19. A. Balla, G. Tuymetova, B. Toth, et al., "Design of Drug-Resistant Alleles of Type-III Phosphatidylinositol 4-Kinases Using Mutagenesis and Molecular Modeling," *Biochemistry* 47 (2008): 1599–1607.

20. O. F. Harraz, T. A. Longden, D. Hill-Eubanks, and M. T. Nelson, "PIP2 Depletion Promotes TRPV4 Channel Activity in Mouse Brain Capillary Endothelial Cells," *eLife* 7 (2018): e38689.

21. Y. Li, R. Mikrani, Y. F. Hu, et al., "Research Progress of Phosphatidylinositol 4-Kinase and Its Inhibitors in Inflammatory Diseases," *European Journal of Pharmacology* 907 (2021): 174300.

22. S. D. Sorensen, D. A. Linseman, E. L. McEwen, A. M. Heacock, and S. K. Fisher, "A Role for a Wortmannin-Sensitive Phosphatidylinositol-4-Kinase in the Endocytosis of Muscarinic Cholinergic Receptors," *Molecular Pharmacology* 53 (1998): 827–836.

23. W. F. Jackson, "Endothelial Ion Channels and Cell-Cell Communication in the Microcirculation," *Frontiers in Physiology* 13 (2022): 805149.

24. F. Gustafsson, H. B. Mikkelsen, B. Arensbak, et al., "Expression of Connexin 37, 40 and 43 in Rat Mesenteric Arterioles and Resistance Arteries," *Histochemistry and Cell Biology* 119 (2003): 139–148.

25. W. H. Evans and L. Leybaert, "Mimetic Peptides as Blockers of Connexin Channel-Facilitated Intercellular Communication," *Cell Communication & Adhesion* 14 (2007): 265–273.

26. A. Nishimura, K. Kitano, J. Takasaki, et al., "Structural Basis for the Specific Inhibition of Heterotrimeric Gq Protein by a Small Molecule," *Proceedings of the National Academy of Sciences of the United States of America* 107 (2010): 13666–13671.

27. M. Fujioka, S. Koda, Y. Morimoto, and K. Biemann, "Structure of FR900359, a Cyclic Depsipeptide From *Ardisia crenata* Sims," *Journal of Organic Chemistry* 53 (1988): 2820–2825.

28. E. M. Pfeil, J. Brands, N. Merten, et al., "Heterotrimeric G Protein Subunit Gαq Is a Master Switch for Gβγ-Mediated Calcium Mobilization by Gi-Coupled GPCRs," *Molecular Cell* 80 (2020): 940–954.e6.

29. D. M. Lehmann, A. M. P. B. Seneviratne, and A. V. Smrcka, "Small Molecule Disruption of G Protein βγ Subunit Signaling Inhibits Neutrophil Chemotaxis and Inflammation," *Molecular Pharmacology* 73 (2008): 410–418.

30. N. H. Carbonetti, "Pertussis Toxin and Adenylate Cyclase Toxin: Key Virulence Factors of Bordetella Pertussis and Cell Biology Tools," *Future Microbiology* 5 (2010): 455–469.

31. J. K. Northup, P. C. Sternweis, M. D. Smigel, L. S. Schleifer, E. M. Ross, and A. G. Gilman, "Purification of the Regulatory Component of Adenylate Cyclase," *Proceedings of the National Academy of Sciences of the United States of America* 77 (1980): 6516–6520.

32. X. Zhu and L. Birnbaumer, "G Protein Subunits and the Stimulation of Phospholipase C by Gs-And Gi-Coupled Receptors: Lack of Receptor Selectivity of Galpha(16) and Evidence for a Synergic Interaction Between Gbeta Gamma and the Alpha Subunit of a Receptor Activated G Protein," *Proceedings of the National Academy of Sciences of the United States of America* 93 (1996): 2827–2831.

33. M. Hohenegger, M. Waldhoer, W. Beindl, et al., "Gsα-Selective G Protein Antagonists," *Proceedings of the National Academy of Sciences* 95 (1998): 346–351.

34. H.-J. Liao and G. Carpenter, "Chapter 110—Phospholipase C," in *Handbook of Cell Signaling*, 2nd ed., ed. R. A. Bradshaw and E. A. Dennis (Academic Press, 2010), 887–891, https://doi.org/10.1016/B978-0-12-374145-5.00110-8.

35. W. M. Oldham and H. E. Hamm, "Heterotrimeric G Protein Activation by G-Protein-Coupled Receptors," *Nature Reviews Molecular Cell Biology* 9 (2008): 60–72.

36. A. P. Campbell and A. V. Smrcka, "Targeting G Protein-Coupled Receptor Signalling by Blocking G Proteins," *Nature Reviews. Drug Discovery* 17 (2018): 789–803.

37. R. Schrage, A. L. Schmitz, E. Gaffal, et al., "The Experimental Power of FR900359 to Study Gq-Regulated Biological Processes," *Nature Communications* 6 (2015): 10156.

38. J. Takasaki, T. Saito, M. Taniguchi, et al., "A Novel Gαq/11-Selective Inhibitor," *Journal of Biological Chemistry* 279 (2004): 47438–47445.

39. U. Pohl, "Connexins: Key Players in the Control of Vascular Plasticity and Function," *Physiological Reviews* 100 (2020): 525–572.

40. M. J. Sanderson, A. C. Charles, and E. R. Dirksen, "Mechanical Stimulation and Intercellular Communication Increases Intracellular Ca2+ in Epithelial Cells," *Cell Regulation* 1 (1990): 585–596.

41. D. Zhu, S. Caveney, G. M. Kidder, and C. C. Naus, "Transfection of C6 Glioma Cells With Connexin 43 cDNA: Analysis of Expression, Intercellular Coupling, and Cell Proliferation," *Proceedings. National Academy of Sciences. United States of America* 88 (1991): 1883–1887.

42. A. C. Charles, C. C. Naus, D. Zhu, G. M. Kidder, E. R. Dirksen, and M. J. Sanderson, "Intercellular Calcium Signaling via Gap Junctions in Glioma Cells," *Journal of Cell Biology* 118 (1992): 195–201.

43. M. Beltramello, V. Piazza, F. F. Bukauskas, T. Pozzan, and F. Mammano, "Impaired Permeability to Ins(1,4,5)P3 in a Mutant Connexin Underlies Recessive Hereditary Deafness," *Nature Cell Biology* 7 (2005): 63–69.

44. C. de Wit, F. Roos, S. S. Bolz, et al., "Impaired Conduction of Vasodilation Along Arterioles in connexin40-Deficient Mice," *Circulation Research* 86 (2000): 649–655.

45. A. M. Simon and A. R. McWhorter, "Decreased Intercellular Dye-Transfer and Downregulation of Non-Ablated Connexins in Aortic Endothelium Deficient in connexin37 or connexin40," *Journal of Cell Science* 116 (2003): 2223–2236.

46. S. E. Wölfle, V. J. Schmidt, B. Hoepfl, et al., "Connexin45 Cannot Replace the Function of Connexin40 in Conducting Endothelium-Dependent Dilations Along Arterioles," *Circulation Research* 101 (2007): 1292–1299.

47. C. de Wit and T. M. Griffith, "Connexins and Gap Junctions in the EDHF Phenomenon and Conducted Vasomotor Responses," *Pflügers Archiv - European Journal of Physiology* 459 (2010): 897–914.

48. L. Leybaert, K. Paemeleire, A. Strahonja, and M. J. Sanderson, "Inositol-Trisphosphate-Dependent Intercellular Calcium Signaling in and Between Astrocytes and Endothelial Cells," *Glia* 24 (1998): 398–407.

49. J. W. Walker, A. V. Somlyo, Y. E. Goldman, A. P. Somlyo, and D. R. Trentham, "Kinetics of Smooth and Skeletal Muscle Activation by Laser Pulse Photolysis of Caged Inositol 1,4,5-Trisphosphate," *Nature* 327 (1987): 249–252.

50. R. Ornelas-Guevara, D. Gil, V. Voorsluijs, and G. Dupont, "Computational Investigation of IP3 Diffusion," *Scientific Reports* 13 (2023): 2922.

51. Y. J. Kim, A. C. Elliott, S. J. Moon, S. I. Lee, and J. T. Seo, "Octanol Blocks Fluid Secretion by Inhibition of Capacitative Calcium Entry in Rat Mandibular Salivary Acinar Cells," *Cell Calcium* 25 (1999): 77–84.

52. C. Faniku, E. O'Shaughnessy, C. Lorraine, et al., "The Connexin Mimetic Peptide Gap27 and Cx43-Knockdown Reveal Differential Roles for Connexin43 in Wound Closure Events in Skin Model Systems," *International Journal of Molecular Sciences* 19 (2018): 604.

53. N. B. Thillaiappan, P. Chakraborty, G. Hasan, and C. W. Taylor, "IP3 Receptors and Ca2+ Entry," *Biochimica et Biophysica Acta (BBA)—Molecular Cell Research* 1866 (2019): 1092–1100.

54. A. A. Khan, J. P. Steiner, M. G. Klein, M. F. Schneider, and S. H. Snyder, "IP3 Receptor: Localization to Plasma Membrane of T Cells and Cocapping With the T Cell Receptor," *Science* 257 (1992): 815–818.

55. C. W. Taylor and O. Dellis, "Plasma Membrane IP3 Receptors," *Biochemical Society Transactions* 34 (2006): 910–912.

56. M. T. Khan, C. D. Bhanumathy, Z. T. Schug, and S. K. Joseph, "Role of Inositol 1,4,5-Trisphosphate Receptors in Apoptosis in DT40 Lymphocytes," *Journal of Biological Chemistry* 282 (2007): 32983–32990.

57. P. Chakraborty, B. K. Deb, V. Arige, et al., "Regulation of Store-Operated Ca^{2+} Entry by IP3 Receptors Independent of Their Ability to Release Ca^{2+}," *eLife* 12 (2022): e80447.

58. A. Bartok, D. Weaver, T. Golenár, et al., "IP_3 Receptor Isoforms Differently Regulate ER-Mitochondrial Contacts and Local Calcium Transfer," *Nature Communications* 10 (2019): 3726.

59. J. Dai, C. Patzke, K. Liakath-Ali, E. Seigneur, and T. C. Südhof, "GluD1 Is a Signal Transduction Device Disguised as an Ionotropic Receptor," *Nature* 595 (2021): 261–265.

60. A. Rodríguez-Moreno and J. Lerma, "Kainate Receptor Modulation of GABA Release Involves a Me Otropic Function," *Neuron* 20 (1998): 1211–1218.

61. A. Zakrzewicz, K. Richter, A. Agné, et al., "Canonical and Novel Non-Canonical Cholinergic Agonists Inhibit ATP-Induced Release of Monocytic Interleukin-1β via Different Combinations of Nicotinic Acetylcholine Receptor Subunits α7, α9 and α10," *Frontiers in Cellular Neuroscience* 11 (2017): 189.

62. L. Jiménez-Pérez, P. Cidad, I. Álvarez-Miguel, et al., "Molecular Determinants of Kv1.3 Potassium Channels-Induced Proliferation," *Journal of Biological Chemistry* 291 (2016): 3569–3580.

63. D. Atlas, "Voltage-Gated Calcium Channels Function as Ca2+−Activated Signaling Receptors," *Trends in Biochemical Sciences* 39 (2014): 45–52.

Supporting Information

Additional supporting information can be found online in the Supporting Information section.